

Tunneling between the Edges of Two Lateral Quantum Hall Systems

W. Kang^{*,§}, H.L. Stormer^{†,§}, K.W. Baldwin[§], L.N. Pfeiffer[§], and K.W. West[§]

**James Franck Institute and Department of Physics, University of Chicago, Chicago, Illinois 60637*

†Department of Physics, Columbia University, New York, New York, 10027

§Bell Laboratories, Lucent Technologies, 600 Mountain Avenue, Murray Hill, NJ 07974

The edge of a two-dimensional electron system (2DES) in a magnetic field consists of one-dimensional (1D) edge-channels that arise from the confining electric field at the edge of the specimen¹⁻³. The crossed electric and magnetic fields, $\mathbf{E} \times \mathbf{B}$, cause electrons to drift parallel to the sample boundary creating a chiral current that travels along the edge in only one direction. Remarkably, in an ideal 2DES in the quantum Hall regime all current flows along the edge⁴⁻⁶. Quantization of the Hall resistance, $R_{xy} = h/Ne^2$, arises from occupation of N 1D edge channels, each contributing a conductance of e^2/h ⁷⁻¹¹. To explore this unusual one-dimensional property of an otherwise two-dimensional system, we have studied tunneling between the edges of 2DESs in the regime of integer quantum Hall effect (QHE). In the presence of an atomically precise, high-quality tunnel barrier, the resultant interaction between the edge states leads to the formation of new energy gaps and an intriguing dispersion relation for electrons traveling along the barrier. The absence of tunneling features due to the electron spin and the persistence of a conductance peak at zero bias are not consistent with a model of weakly interacting edge states.

The edge channels of the QHE is a prototypical one-dimensional electronic system. Other such one-dimensional model systems include semiconductor based quantum wires¹², carbon nanotubes^{13,14}, and molecular chain materials¹⁵. While these systems force the electrons to move along a preferential direction, the edge channels of a QHE system is unique in its ability to adjust itself spatially as well as energetically. A localized defect is easily avoided by the edge current by simply skirting the impurity potential. In real samples, variations in the potential landscape can generate a complex and intriguing topology of edge channels^{16,17}. Consequently, most real edge channels are ill defined, both spatially and energetically, and it becomes difficult to generalize various experimental geometries in terms of 1D edge states. While typical experiments seek to study edge states in *lithographically defined* geometries^{18–19}, their edges typically fluctuate on the scale of a magnetic length. In order to address the energetics of edge channels, well-defined geometries with clearly delineated edges are essential. In particular for tunneling experiments, where distance factors exponentially into the tunneling current, exact knowledge of the shape and the magnitude of the barrier is crucial in making contact with model calculations.

Our 2DES-barrier-2DES (2D-2D) tunneling device consists of two stripes of 2DESs separated by an atomically precise 88Å-thick semiconductor barrier, fabricated by cleaved edge overgrowth, as shown in Fig.1a. We explore the lateral tunneling between these two physically separated 2DESs in the QHE regime. Fig.1c shows the differential conductance of the high density sample at 9.2T and 6.0T. At 9.2T, dI/dV_{bias} is strongly suppressed around zero bias, while oscillatory conductance peaks appear above a threshold electric field. Each peak represents the onset of an additional tunneling path through the barrier. Successive conductance peaks are nearly equally spaced with a spacing on the order of the cyclotron energy $\hbar\omega_c$ ($\sim 17\text{meV}$ at 10T) and the amplitude of their oscillation decreases. Most of the dI/dV_{bias} -traces resemble the 9.2T conductance data. However, for certain ranges of magnetic fields, there is no threshold to tunneling and a very sharp and tall conductance peak arises at zero bias, as illustrated by the 6T data.

Fig.2 shows an image map of the dI/dV_{bias} data as a function of Landau level filling factor, $\nu = nh/eB$, and the normalized bias voltage, $eV_{peak}/\hbar\omega_c$. Blue and red represent small and large dI/dV_{bias} signals, respectively. With scaled axes, the disparate data from two different samples with very different electron densities join and produce a universal tunneling map for the 2D-2D tunneling. Altogether, an intriguing pattern arises with a continuous progression of conductance maxima (black squares and circles) from the low density to the high density data. The dI/dV_{bias} plot exhibits gap-like thresholds that define regions of vanishing dI/dV_{bias} in which the tunneling is strongly suppressed. Around zero bias, tunneling is suppressed in a bell-shaped region for filling factors $\nu < 1$. Similar thresholds occur at higher fillings near $\nu \sim 2$. Between fillings $\nu = 1.2 - 1.5$ and $2.2 - 2.5$, a sharp conductance peak dominates at zero bias. The positions of the oscillatory conductance peaks vary roughly linearly at high fillings and produce a fan of maxima that branches out from zero bias. Some of these branches cross each other above $\nu > 1$. For fillings $\nu < 1$ the different branches tend to saturate.

In analogy to the edge-state transport in the QHE, we consider the 2D-2D tunneling in terms of 1D edge states in the presence of a barrier. The edge states around the perimeter of the 2D-2D system are the same as in a simple 2DES, whose dispersion relation along the edge is approximately parabolic. This is no longer the case along the barrier. Fig. 3a illustrates the spatial dependence of the Landau level energy in its vicinity. The energy levels $E(x)$ of Fig. 3a correspond to the energy of an electron with orbit guiding center x . Since $x = -k_y\ell_o^2$, the energy diagram of Fig. 3a is also the 1D *dispersion relation*, $E(k_y)$, for electrons traveling *along* the barrier in the y-direction with velocity $v = \hbar^{-1}dE/dk_y = \hbar^{-1}\ell_o^2dE(x)/dx$. Electrons on the left side of the barrier counter-propagate with respect to those on the right side of the barrier. At the intersections of the two sets of rising Landau ladders, there exist two oppositely traveling, degenerate edge states with the same wavevector, $k_y = -x/\ell_o^2$. The degeneracy at the crossings is lifted by the formation of a series of small energy gaps that separate the symmetric and antisymmetric combinations of the underlying wavefunctions as seen in Fig. 3a. Altogether, Fig 3a bears a surprising resemblance with the data of Fig. 2.

Electronic transport *along* the barrier depends crucially on the position of the Fermi energy with respect to this complex 1D barrier level structure^{20,21}. When the Fermi level resides below the first maximum, say at E_1 in Fig. 3a, electrons in both 2DESs follow two separate, counter-propagating tracks along the junction as depicted in inset A of Fig. 3a. Although traveling along the barrier, they have very different k_y -wave vectors and are practically uncoupled. Therefore, tunneling through the barrier is negligible, corresponding to the absence of a peak at zero bias at low filling factor.

As the Fermi level reaches the first maximum at E_2 , the edge states on both sides of the barrier have identical wavevector and resonate, which leads to substantial tunneling. In fact, the tracks of the wavefunctions have insignificantly changed as compared to inset A, but coupling between both edges has vastly increased due to the equivalence of their k_y -momentum. Consequently, at this particular position of E_F , the conductance at zero bias turns finite, as observed in the zero bias peak of our data. According to the barrier level scheme in Fig. 3a, the edge states from the second Landau level, $N = 1$, are also occupied for this range of fillings, but remain uncoupled.

As the Fermi level rises slightly above this critical position and into the gap of the dispersion relation, electrons can no longer travel *along* the barrier, as shown in the inset B of Fig. 3a. Consequently, coupling between both 2DESs should vanish and tunneling should cease. This represents an interesting paradox. If electrons can no longer travel along the barrier and, due to the chirality of the edge channel, are not allowed to backscatter, one would think they *need* to tunnel. This should give rise to a conductance of $\sim e^2/h$, which is, however, two orders of magnitude larger than observed. The detailed tunneling and scattering model at this position of E_F remains unclear. In any case, our model does not seem to agree with experiment, in which the zero-bias peak persists for a range of filling factors $1.2 < \nu < 1.5$, rather than existing at just one B-field. This may be related to electron scattering along the barrier, which relaxes k-conservation and washes out the dispersion relation. It is also unclear why the conductance vanishes abruptly at $\nu \sim 1.5$. This may coincide with E_F reaching the top of the energy gap of the $N = 0$ branch, where

both 2DESs couple once again along the barrier. A sharp zero-bias conduction and a strong suppression of tunneling alternate as E_F moves through the higher lying gaps in Fig. 3a.

What is the origin of the complex overall pattern of Fig. 2, away from $V_{bias} = 0$, and what is its relationship to Fig. 3a? At finite bias, one set of Landau levels of Fig. 3a is raised with respect to the other by an energy eV_{bias} , as shown in Fig. 3b. This results in a shift of the intercepts and the conditions for onset of conduction is moved to a different energy. For example, when $E_F = E_1$ in Fig. 3a, tunneling across the barrier is inhibited, due to the absence of coupling of the edge states. In Fig. 3b the application of eV_{bias} has shifted the crossing so as to coincide with E_1 . This immensely enhances the coupling between both 2DESs in analogy to position E_2 in Fig. 3a and provides an explanation for the shift of the onset of tunneling to higher V_{bias} for smaller ν in Fig. 2.

In general, whenever the Fermi energy coincides with one of the crossing points, electrons can tunnel through the barrier and relax to the Fermi energy of the 2DES, lying eV_{bias} below. Each additional coincidence of the levels produces a peak in dI/dV_{bias} . We can track their positions if we neglect the small gaps at the crossings. The Landau ladders on both sides are approximately described by

$$\begin{aligned} \frac{E_L}{\hbar\omega_c} &= \left(\frac{x}{\ell_o} + \sqrt{N_L + 1} \right)^2 + (N_L + \frac{1}{2}) \\ \text{and} \\ \frac{E_R}{\hbar\omega_c} &= \left(\frac{x}{\ell_o} - \sqrt{N_R + 1} \right)^2 + (N_R + \frac{1}{2}) - \frac{eV_{bias}}{\hbar\omega_c} \end{aligned} \quad (1)$$

continued by flat Landau levels for $\frac{x}{\ell_o} \geq \sqrt{N+1}$. Neglecting N_R and N_L versus $eV_{bias}/2\hbar\omega_c$, which is justified for large sections of Fig. 2, and assuming that $\frac{E_L}{\hbar\omega_c} \approx \nu$, which holds for very broad Landau levels, as is likely the case in our lower-mobility specimen, we arrive at

$$\nu \approx \left(\frac{eV_{bias}}{2\hbar\omega_c} + \sqrt{N_L + 1} \right)^2 + (N_L + \frac{1}{2}). \quad (2)$$

as the condition for coincidence. Eq. 1, which, together with its $L-R$ mirror image describes the barrier level structure of Fig. 3a, is identical to eq. 2, which identifies the peaks in the differential conductance in Fig. 2 as long as $\frac{E_L}{\hbar\omega_c}$ is replaced by ν and x/ℓ_o is replaced by $eV_{bias}/2\hbar\omega_c$. This resolves the puzzle of the intriguing similarity between both graphs.

While we can account for the general features of our experimental results, many aspects of the data remain unresolved and require an explanation beyond our simple model. One such feature is the extended existence of the zero-bias peak, which is expected to occur only at the point of coincidence of E_F with the edges of the gaps. The origin of this discrepancy may be a relaxed k -conservation due to remnant disorder along the barrier, which scatters electrons, broadens the dispersion relation and therefore extends the allowed energy range for strong tunneling. Such a broadening may also account for the conductance which is much reduced compared to e^2/h : The sharp resonance with universal conductance is broadened into a band of much lower, average conductance. However, the sharpness of the zero-bias peak as a function of voltage bias implies limited broadening. A proper accounting of the role of disorder in 2D-2D tunneling requires a detailed, quantitative analysis of our 2D-2D device.

Another puzzling feature of our data is the position in filling factor at which the zero bias conductance peak appears. According to Fig. 3a, the first coincidence of the Landau ladders occurs at $\nu > 4$, somewhat above the $N = 1$ Landau level, contrary to the experimental value of $\nu \approx 1.2$. Similarly, the next coincidence is expected for $\nu > 6$, while it is observed at $\nu \sim 2.2$. These observations point to a shifting of the levels in addition to a possible broadening. It could arise from self-consistent screening and from an accumulation of charge in the vicinity of the barrier²², which modifies the level scheme.

Finally, the influence of the electron spin on our experiment as well as on the dispersion relation in Fig. 3a remains unclear. While the Zeeman splitting in GaAs is only $1/70$ of the cyclotron splitting, partial and spatially dependent occupation of Landau levels near the barrier can produce large spatially dependent enhancement of the g -factor^{1,2}. This can give rise to additional coincidences – possibly over ranges of fillings – and will appear in the tunneling characteristics, in particular, if spin-flip scattering is strong. This absence of spin-dependent features in the tunneling data remains a key puzzle. Numerical studies of our comparably simple physical system should provide guidance as to the relative importance

of different mechanisms.

-
1. Prange, R.E. & Girvin, S.M. (eds) *The Quantum Hall Effect* 2nd edn (Springer, New York, 1990).
 2. Das Sarma, S. & Pinczuk, A. (eds) *Perspectives in Quantum Hall Effects* (Wiley Inter-Science, New York, 1997).
 3. Halperin, B.I. Quantized Hall conductance, current-carrying edge states, and the existence of extended states in a two-dimensional disordered potential. *Phys. Rev. B* **25**, 2185-2188 (1983).
 4. MacDonald, A.H. & Streda, P. Quantized Hall effect and edge currents. *Phys. Rev. B* **29**, 1616-1619 (1984).
 5. Apenko, S.M. & Lozovik, Yu. E. J. The quantized Hall effect in strong magnetic fields. *Phys. C* **18**, 1197-1203 (1985).
 6. Fontein, P.F. et al. Spatial potential distribution in GaAs/Al_xGa_{1-x}As heterostructures under quantum Hall conditions studied with the linear electro-optic effect. *Phys. Rev. B* **43**, 12090-3 (1991).
 7. Buttiker, M. Absence of backscattering in the quantum Hall effect in multiprobe conductors. *Phys. Rev. B* **38**, 9375-9389 (1988).
 8. Streda, P., Kucera, J. & MacDonald, A.H. Edge states, transmission matrices, and the Hall resistance. *Phys. Rev. Lett.* **59**, 1973-1975 (1987).
 9. Jain, J.K. & Kivelson, S.A. Landauer-type formulation of quantum-Hall transport: critical currents and narrow channels. *Phys. Rev. B* **37**, 4276-4279 (1988).
 10. Haug, R.J., MacDonald, A.H., Streda, P. & von Klitzing. Quantized multichannel magnetotransport through a barrier in two dimensions. *Phys. Rev. Lett.* **61**, 2797-2800 (1988).
 11. Washburn, S., Fowler, A.B., Schmid, H. & Kern, D. Quantized Hall effect in the presence of backscattering. *Phys. Rev. Lett.* **61**, 2801-2804 (1988).
 12. Yacoby, A. et al. Non-universal conductance quantization in quantum wires. *Phys.*

Rev. Lett. **77**, 4612-4615 (1996).

13. Wildoer, J.W. G., Venema, L.C., Rinzler, A.G., Smalley, & R.E., Dekker, C. Electronic structure of atomically resolved carbon nanotubes. *Nature* **391**, 59-62 (1998).

14. Odom, T.W., Huang, J., Kim, P. & Lieber, C.M. Atomic structure and electronic properties of single walled carbon nanotubes. *Nature* **391**, 62-64 (1998).

15. Ishiguro, T., Yamaji, K., & Saito, G. *Organic Superconductors* 2nd edn (Springer- Verlag, New York, 1998).

16. Tessmer, S.H., Glicofridis, P.I., Ashoori, R.C., Levitov, L.S., & Melloch, M.R. Surface charge accumulation imaging of a quantum Hall liquids. *Nature*. **392**, 51-54 (1998).

17. McCormick, K.L. et. al. Scanned potential microscopy of edge and bulk currents in the quantum Hall regime. *Phys. Rev. B* **59**, 4654 (1999).

18. Goldman, V.J. & Su, B. Resonant tunneling in the quantum Hall regime: measurement of fractional charge. *Science* **267**, 1010-12 (1995).

19. Tarucha, S., Honda, T., & Saku, T. Reduction of quantized conductance at low temperatures observed in 2 to 10 μm -long quantum wires. *Solid State Communications*, **94**, 413-18 (1995).

20. Ho, T.L. Oscillatory tunneling between quantum Hall systems. *Phys. Rev. B* **50**, 4524-4533 (1994).

21. Girvin, S.M. Private Communication.

22. Wulf, U., Gudmundsson, V. & Gerhardts, R.R. Screening properties of the two- dimensional electron gas in the quantum Hall regime. *Phys. Rev. B*. **38**, 4218-4230 (1988).

23. Pfeiffer, L.N. et. al. Formation of a high quality two-dimensional electron gas on cleaved GaAs. *Appl. Phys. Lett* **56**, 1697-1699 (1990).

24. Chang, A.M., Pfeiffer, L.N., & West, K.W. Observation of chiral Luttinger behavior in electron tunneling into fractional quantum Hall edges. *Phys. Rev. Lett.* **77**, 2538-2341 (1996).

We are very grateful to S.M. Girvin for providing us with much insight into the intricate energetics of our experimental geometry. We would also like to thank R. De Picciotto, A. M. Chang, T.L. Ho, and J.P. Eisenstein for valuable discussions.

Correspondence and requests for materials should be addressed to W.K.(e-mail: wkang@rainbow.uchicago.edu).

Fig. 1. Structure and differential conductance measurement of the 2D-2D tunneling device. (a). The junctions are fabricated by cleaved edge overgrowth in molecular beam epitaxy (MBE)^{23,24}. The first growth on a standard (100) GaAs substrate consists of an undoped $13\mu m$ GaAs layer followed by a 88\AA -thick digital alloy of undoped $\text{Al}_{0.1}\text{Ga}_{0.9}\text{As}/\text{AlAs}$, and completed by a $14\mu m$ layer of undoped GaAs. This triple-layer sample is cleaved along the (110) plane in an MBE machine and a modulation-doping sequence is grown over the exposed edge. It consists of a 3500\AA -thick AlGaAs layer, delta-doped with Si at a distance of 500\AA from the interface. Carriers from the Si impurities transfer only into the GaAs layers of the cleaved edge, forming two stripes of 2DESs of width $13\mu m$ and $14\mu m$ separated from each other by a 88\AA -thick, $\text{Al}_{0.1}\text{Ga}_{0.9}\text{As}/\text{AlAs}$ barrier. The sample is fabricated into a mesa incorporating the barrier and the two 2DESs. Contacts are made to the 2DESs, far away from the tunneling region. (b) Schematic band structure of the 2D-2D tunneling device. Two different samples with electron density of $n = 1.1 \times 10^{11}\text{cm}^{-2}$ and $n = 2.0 \times 10^{11}\text{cm}^{-2}$ are studied. From a simultaneously grown monitor wafer we estimate the mobility of the 2DESs in the device to be $\sim 1 \times 10^5\text{cm}^2/V\text{sec}$. (c) Two representative traces of differential conductance through the tunneling barrier with electron density $n = 2.0 \times 10^{11}\text{cm}^{-2}$. A low-frequency AC-technique (typically $10\mu V$ amplitude) is employed to measure the differential conductance, dI/dV_{bias} , through the barrier in the presence of a DC voltage bias, V_{bias} . The samples are measured at $T = 300\text{mK}$ in a magnetic field. Near zero bias differential conductances, dI/dV_{bias} , nearly vanish, while conductance oscillations on the order of $10^{-6}\Omega^{-1}$ are found at high bias.

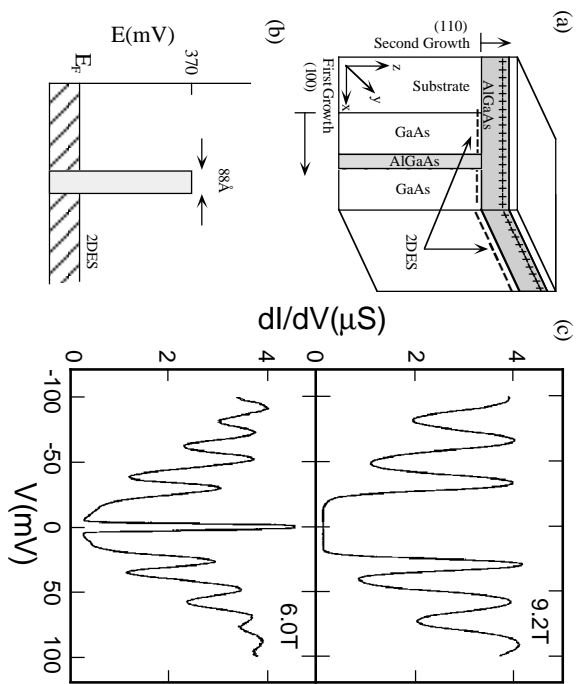
Fig. 2. Evolution of differential conductance of 2D-2D tunneling devices under high magnetic fields. The Landau level filling factor, $\nu = nh/eB$, and the normalized bias, $eV_{peak}/\hbar\omega_c$, are used as universal axis for the 2D-2D tunneling data from samples with electron densities, $n = 2.0 \times 10^{11} \text{cm}^{-2}$ (top) and $n = 1.1 \times 10^{11} \text{cm}^{-2}$ (bottom). Their maxima are indicated by black circles and squares, respectively. Blue (red) regions represent minimum (maximum) conductance. In the blue region, conductances, dI/dV_{bias} , nearly vanish, while the red areas represent conductances on the order of $10^{-6} \Omega^{-1}$.

Fig. 3. Schematic energy dependence of the Landau levels in the vicinity of the barrier. (a). Shown for zero voltage bias. Far away from the barrier Landau levels are equally spaced, $E_N = (N + 1/2)\hbar\omega_c$. As electrons approach the edge or the barrier their energy rises parabolically.

$$\frac{E}{\hbar\omega_c} = \left(\left| \frac{x}{\ell_o} \right| + \sqrt{N+1} \right)^2 + \left(N + \frac{1}{2} \right), N = 0, 1, 2, \dots \text{ and } \left| \frac{x}{\ell_o} \right| \leq \sqrt{N+1},$$

otherwise

$\frac{E}{\hbar\omega_c} = N + \frac{1}{2}$ where $\ell_o = \sqrt{eB/h}$ is the magnetic length. In the vicinity of the barrier, these parabolas anti-cross and create a gapped spectrum. The traces represent the energy of an electron whose guiding center is located at x . N is the Landau level index, E_1 through E_3 represent Fermi energies at different filling factors. Inserts represent the in-plane track of the electronic wavefunction. (b) Same as Fig. 3a but with a bias of $\sim 2\hbar\omega_c$ applied across the barrier.



This figure "fig2a.jpg" is available in "jpg" format from:

<http://arxiv.org/ps/cond-mat/9910205v1>

This figure "fig3.jpg" is available in "jpg" format from:

<http://arxiv.org/ps/cond-mat/9910205v1>